Temperature Dependence of Vibrational Energy Transfer in a Protein Molecule

Kei Moritsugu,[†,‡] Osamu Miyashita,[‡,§] and Akinori Kidera*[,†]

Graduate School of Integrated Science, Yokohama City University, Tsurumi-ku, Yokohama 230-0045, Japan, Department of Chemistry, Graduate School of Science, Kyoto University, Sakyo-ku, Kyoto 606-8502, Japan, and Center for Theoretical Biological Physics and Department of Physics, University of California at San Diego, 9500 Gilman Drive, La Jolla, California 92093

Received: December 25, 2002

The anharmonic dynamics of a protein molecule was studied by molecular dynamics simulations of the intramolecular vibrational energy transfer in myoglobin. A small excess kinetic energy was added to a specified normal mode, and the process of the energy transfer to other modes was observed. It was found that the vibrational energy was transferred by two distinct mechanisms depending on temperature. Near zero temperature, the vibrational energy is transferred as a process of the Fermi resonance mostly through the third-order coupling terms from one mode to only a limited number of modes, satisfying the resonance condition. As the temperature increases, the resonance-type transfer is dominated by the off-resonance energy transfer through various mode-coupling terms. Near room temperature, the energy transfer involves higher-order coupling terms and indirect processes through intermediate modes in addition to the transfers through the lower-order couplings. In the short-time limit immediately after starting the energy-transfer simulation, we can observe the direct energy transfer between a pair of modes, which shows the dominance of the lower-order coupling terms, and the influence from the dynamic transition at about 180 K.

1. Introduction

The biological function of a protein can be explained by a physicochemical picture in which a series of switching motions, triggered in response to external factors such as ligand binding, couple with each corresponding chemical reaction to the ligand. The switching motions, or the structural transitions between the resting and the activated states, are the consequence of the highly anharmonic dynamics on the rugged potential surface of the protein molecule.[1,2]

Molecular dynamics (MD) simulation has been a powerful tool used to study the anharmonic dynamics of proteins. One of the most successful models for analyzing the anharmonic dynamics in MD trajectories is the one based on the quasiharmonic approximation, where the distribution function is approximated up to the second-order moments.[3,4] The anharmonicity is highlighted by the deconvolution of the second moments into the short-time harmonic vibrations and the long-time anharmonic motions.[5] Although this model analyzes the equilibrium distribution function, it is not suitable for the analysis of the response or the relaxation behavior.

As the first stage for understanding the anharmonicity in the time domain of protein motions, we adopted an assumption that protein motions can be described by a system of perturbed harmonic oscillators:

$$L = \sum_{i=1}^{N}\left(\frac{1}{2}\dot{q}_i^2 - \frac{1}{2}\omega_i^2 q_i^2\right) - \sum_{i,j,k=1}^{N} \alpha_{ijk} q_i q_j q_k - \sum_{i,j,k,l=1}^{N} \beta_{ijkl} q_i q_j q_k q_l - \cdots \quad (1)$$

where L is the Lagrangian of the system, q_i is the mass-weighted coordinates of the ith normal mode, ω_i is its frequency, and N is the number of internal degrees of freedom in the system. The external field is not considered here. The higher-order terms with coefficients α_{ijk}, β_{ijkl},... represent the perturbation of the harmonic part of the Lagrangian or the mode couplings. Through these coupling terms, the vibrational energy is transferred among normal modes. In other words, the anharmonic part of the dynamics can be explained by tracing the vibrational energy transfer from one mode to another.

In our previous study, we investigated a simple case near zero temperature.[6] It was found that the vibrational energy was transferred from a normal mode to few normal modes that were selected by the frequency relation of the Fermi resonance and the magnitude of the third-order mode coupling term. It was confirmed that the magnitude of the coupling coefficients was mainly determined by the degree of geometrical overlap of the corresponding normal modes.

In this article, we studied the vibrational energy transfer at various temperatures. It has been shown in theoretical studies on the "intramolecular energy redistribution"[7−10] that at low temperatures the lower-order coupling terms dominate the energy transfer but with increasing temperature the transfer due to the higher-order coupling terms or the indirect transfer via intermediate modes becomes significant. To analyze such

* Corresponding author. E-mail: kidera@tsurumi.yokohama-cu.ac.jp. Tel: 81-45-508-7231. Fax: 81-45-508-7363.
† Yokohama City University.
‡ Kyoto University.
§ University of California at San Diego.

10.1021/jp027823q CCC: $25.00
Published on Web 03/18/2003

complicated processes at higher temperatures, we focused on the transfer process in a short-time limit, where we can observe the direct transfer process exclusively.

Another important issue in the temperature dependence of protein dynamics is the glass transitionlike phenomena around 200 K.[11−17] It is considered that below the transition temperature a protein molecule is confined in one of the conformational substates and the motions are more or less vibrational. Above the transition temperature, the protein attains sufficient kinetic energy to cross over energy barriers between the substates, and it starts to move in a diffusive manner. Here, we investigate how the influence from the dynamic transition appears in the vibrational energy transfer.

2. Theory and Methods

2.1. Simulation System and Calculations. We carried out a molecular dynamics (MD) simulation of deoxymyoglobin (pdb entry: 1mwd; 2475 atoms), where a specified mode (we call it a perturbed mode) was exclusively assigned a small excess of vibrational energy. From the simulation data, we then observed how the excess vibrational energy of the perturbed mode becomes transferred to other modes or how the normal modes are coupled with each other. Here, we chose mode 2861, whose frequency is 827.2 cm^{-1}, as the perturbed mode because the frequency is in the same range as the vibrational mode of the heme group, which has been studied by many authors.[17−26] The MD simulations were performed under the microcanonical condition with a time step of 0.5 or 0.1 fs using the program PRESTO[27] with the AMBER force fields for all atoms.[28] The shorter time step, 0.1 fs, was used in the analysis of the short-time behavior within 1 fs. No explicit solvent molecule was considered, and the distance-dependent dielectric constant ($\epsilon = 2r$; r is the interatomic distance) was used. No constraint was imposed. The normal modes of myoglobin were calculated by diagonalizing a Hessian matrix after an energy minimization of the pdb coordinates.[29] Using the eigenvector matrix thus derived, the MD trajectories were converted into the normal coordinates and the corresponding momenta. The numbering scheme of the normal modes of myoglobin is 7 for the lowest-frequency internal mode of 5.4 cm^{-1} and 7425 for the highest-frequency mode of 3712.3 cm^{-1}.

2.2. Analytical Derivation of Energy Transfer between Two Oscillators. Here, we present an analytical solution for the third- and fourth-order coupling between a pair of oscillators in the classical form, which will be the basis for understanding the simulation results. The following solution can easily be extended to a system having higher-order coupling and including more than three oscillators.

The Lagrangian of the model system is written as

$$L = \frac{1}{2}(\dot{q}_1^2 + \dot{q}_2^2) - \frac{1}{2}(\omega_1^2 q_1^2 + \omega_2^2 q_2^2) - \alpha q_1^2 q_2 \qquad (2)$$

The corresponding equations of motion are

$$\ddot{q}_1 = -\omega_1^2 q_1 - 2\alpha q_1 q_2$$
$$\ddot{q}_2 = -\omega_2^2 q_2 - \alpha q_1^2 \qquad (3)$$

The solution of eq 3, up to first order in α, is given by

$$q_1 = A_1 \cos\tau_1 - \alpha A_1 A_2 \left[\frac{\cos(\tau_1+\tau_2)}{\omega_1^2 - (\Omega_1+\Omega_2)^2} + \frac{\cos(\tau_1-\tau_2)}{\omega_1^2 - (\Omega_1-\Omega_2)^2}\right] + O(\alpha^2)$$

$$q_2 = A_2 \cos\tau_2 - \frac{\alpha A_1^2}{2}\left(\frac{\cos 2\tau_1}{\omega_2^2 - 4\Omega_1^2} + \frac{1}{\omega_2^2}\right) + O(\alpha^2) \qquad (4)$$

where Ω_i is the modulated frequency [$\Omega_i = \omega_i + O(\alpha)$] due to the perturbation and $\tau_i = \Omega_i t + \theta_i$ with θ_i being the initial phase. The total energy of each mode in the harmonic approximation, $(\dot{q}_i^2 + \omega_i^2 q_i^2)/2$, is given by eq 5 when the frequency modulation is ignored, namely, $\Omega_i \simeq \omega_i$.

$$E_1 \simeq \frac{1}{2}A_1^2\omega_1^2 - \frac{\alpha A_1^2 A_2}{4}\left[\frac{2\omega_1}{2\omega_1+\omega_2}\cos(2\tau_1+\tau_2) + \frac{2\omega_1}{2\omega_1-\omega_2}\cos(2\tau_1-\tau_2)\right] + O(\alpha^2)$$

$$E_2 \simeq \frac{1}{2}A_2^2\omega_2^2 - \frac{\alpha A_1^2 A_2}{4}\left[\frac{\omega_2}{2\omega_1+\omega_2}\cos(2\tau_1+\tau_2) - \frac{\omega_2}{2\omega_1-\omega_2}\cos(2\tau_1-\tau_2) + 2\cos\tau_2\right] + O(\alpha^2) \qquad (5)$$

From these equations, it can be confirmed that the total energy is maintained at the first order of α (i.e., $E_1 + E_2 + \alpha q_1^2 q_2 =$ const).

When the resonance condition is satisfied, $2\omega_1 - \omega_2 \equiv \Delta_0 \sim O(\alpha)$, it is shown in the following equations that the coupling term makes a significant contribution to the zeroth order of α.[30]

$$E_1 \simeq \frac{1}{2}A_1^2\omega_1^2 - \frac{\alpha}{\Delta_0}\frac{A_1^2 A_2 \omega_1}{2}\cos(2\tau_1-\tau_2) + O(\alpha)$$

$$E_2 \simeq \frac{1}{2}A_2^2\omega_2^2 + \frac{\alpha}{\Delta_0}\frac{A_1^2 A_2 \omega_2}{4}\cos(2\tau_1-\tau_2) + O(\alpha) \qquad (6)$$

In this case, the energy conservation is satisfied at the zeroth order of α (i.e., $E_1 + E_2 =$ const). A characteristic feature of the resonance behavior is that the time course of the energy transfer has a much longer period, $2\pi/\Delta_0$, compared to the frequencies of the two modes.

However, within a very short time after the perturbation [$\Delta t \ll 2\pi/(2\omega_1 + \omega_2)$], eq 5, to first order in α, becomes

$$E_1(\Delta t) - E_1(0) = \frac{\alpha A_1^2 A_2}{2}\omega_1 \Delta t[\sin(2\theta_1+\theta_2) + \sin(2\theta_1-\theta_2)]$$

$$E_2(\Delta t) - E_2(0) = \frac{\alpha A_1^2 A_2}{4}\omega_2 \Delta t[\sin(2\theta_1+\theta_2) - \sin(2\theta_1-\theta_2) + 2\sin\theta_2] \qquad (7)$$

The selection mechanism of the resonance does not work within Δt because the denominator, $2\omega_1 - \omega_2$, in eq 5 disappears in eq 7. Therefore, in a very short time, the energy transfer occurs in the off-resonance mechanism and is governed by the mode coupling whose magnitude is proportional to the coupling constant α.

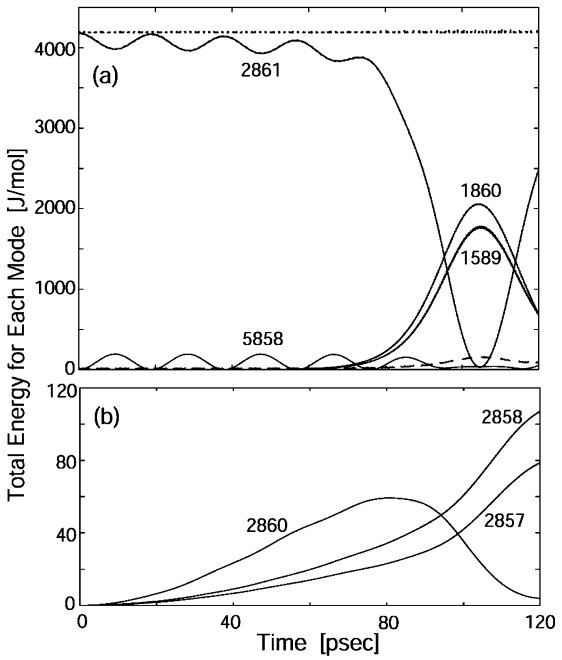

Figure 1. Time course of the total energy after the perturbation for seven modes: (a) the perturbed mode 2861 and the resonance modes 1589, 1860, 5858 of the third-order coupling and (b) the resonance modes 2857, 2858, 2860 of the fourth-order coupling. The sum of the total energy for the other 7412 modes (− −) and that for the whole modes (••) are also shown in a.

In a system with large degrees of freedom at high temperature, it is expected that the energy transfer of the off-resonance type (eq 7) will dissipate the perturbed energy to a number of modes before the resonance-type transfer (eq 6) occurs at $t \geq 2\pi/\Delta_0$. This is the reason for the change in the mechanism of the energy transfer from resonance to off-resonance at higher temperatures. Even in a system with more than two degrees of freedom, eq 7 may give an accurate estimation of the direct energy transfer between modes 1 and 2 when Δt is small enough for the other modes not to disturb the energy state of modes 1 and 2. For such a small value of Δt, it is possible to ignore the indirect transfer through the intermediate modes.

3. Results and Discussion

3.1. Energy Transfer Near Zero Temperature. Here, we describe the energy transfer near zero temperature through the third- and fourth-order coupling terms. Figure 1 shows the time course of the total energy after the perturbation of myoglobin. This trajectory was obtained by an MD simulation with the initial condition in which the minimum-energy structure at 0 K was perturbed by kinetic energy of 1 kcal/mol (1 kcal/mol = 4.184 kJ/mol) imposed on mode 2861 (its frequency is 827.2 cm^{-1}). The temperature after the equipartition of the perturbed energy corresponds to 0.136 K (i.e., near zero). This system is characterized as weakly anharmonic, as seen in the sum of the harmonic total energy, $\sum_i[(\dot{q}_i^2 + \omega_i^2 q_i^2)/2]$, showing no drift. The result clearly indicates that the energy transfer occurred in the mechanism of the Fermi resonance of the third- and fourth-order coupling terms. The perturbed energy of mode 2861 is transferred to modes 1589 (362.9 cm^{-1}), 1860 (464.5 cm^{-1}), and 5858 (1654.5 cm^{-1}) through the third-order coupling and to modes 2857 (826.9 cm^{-1}), 2858 (827.0 cm^{-1}), and 2860 (827.1 cm^{-1}) through the fourth-order coupling. The energy transferred to the other 7412 modes is negligibly small, as shown in the Figure.

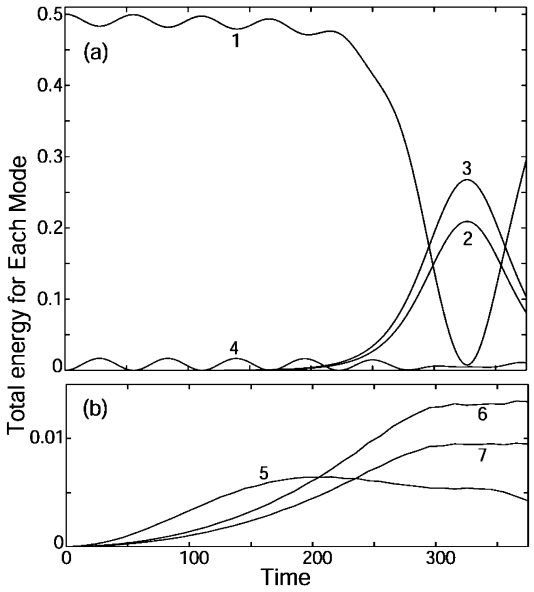

Figure 2. Time course of the total energy after the perturbation to mode 1 for seven oscillators in the model system. See the text for details.

Figure 1a shows two different types of third-order coupling: two modes (2861 and 5858) couple in the term $\alpha_1 q_{2861}^2 q_{5858}$, satisfying the resonance condition 827.2 $cm^{-1} \times 2 \approx 1654.5$ cm^{-1} (type 1), and three modes (2861, 1589, and 1860) couple in the term $\alpha_2 q_{2861} q_{1589} q_{1860}$, whose resonance condition is 827.2 $cm^{-1} \approx 362.9$ $cm^{-1} + 464.5$ cm^{-1} (type 2). It is also shown that the energy transfer via type 2 occurred earlier than that via type 1. This is explained as follows. At $t = 0$, all of the amplitudes besides q_{2861} are zero. Hence, the coupling term of type 1, $\alpha_1 q_{2861}^2 q_{5858}$, gives a nonzero force, $-\partial L/\partial q_{5858}$, to excite mode 5858. The other modes require a longer period, ~80 ps, to be excited indirectly, probably through the low-frequency modes.

Figure 1b shows the energy transfer through the fourth-order coupling terms, which is much smaller than the transfer by the third-order terms, as expected in eq 1. In the fourth-order coupling between a pair of modes, there are two major types, $\beta_3 q_{2861}^3 q_i$(type 3) and $\beta_4 q_{2861}^2 q_i^2$(type 4), both of which are characterized by the resonance condition $\omega_i \approx \omega_{2861}$. Although these two types having the same resonance condition cannot be distinguished from each other, it is expected that type 3 occurs prior to type 4 because type 3 gives a nonzero force to mode q_i but type 4 does not. The contribution from the other fourth-order coupling term, $\beta_5 q_{2861} q_i^3$, is expected to be much smaller than those from type 3 and type 4 and thus will not be discussed here.

To confirm the above assignments of the transferred energy to each coupling term, we performed an MD simulation of a model system with seven weakly coupled harmonic oscillators. Oscillators 1 ($\omega_1 = 5.385$) and 2 ($\omega_2 = 10.779$) are coupled with type 1 ($\alpha_1 = 0.12$), and oscillators 1, 3 ($\omega_3 = 2.362$), and 4 ($\omega_4 = 3.024$) are coupled with type 2 ($\alpha_2 = -0.13$). In addition, oscillators 1 and 5 ($\omega_5 = 5.3848$), 1 and 6 ($\omega_6 = 5.3844$), and 1 and 7 ($\omega_7 = 5.3843$) are coupled with type 3 ($\beta_3 = 0.025$, 0.014, and 0.012, respectively) and type 4 ($\beta_4 = 0.40$, 0.16, and 0.12, respectively). These frequencies are those of the real values scaled by ~0.0065. The coupling coefficients were chosen so that the system may reproduce the behavior in Figure 1. Figure 2 shows the result of the MD simulation of the model system, reproducing the behavior in Figure 1 almost perfectly.

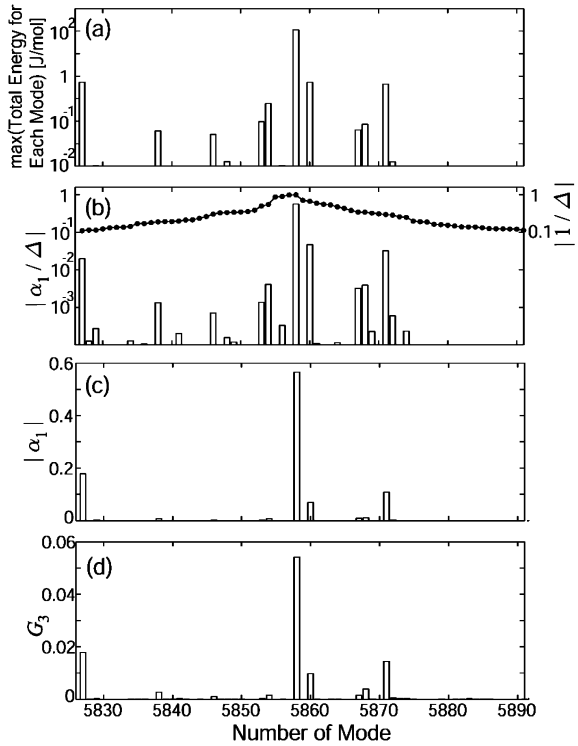

Figure 3. Comparison of various quantities for the energy transfer of type 1 plotted against the mode number around resonance mode 5858. (a) Maximum of the total energy observed in the simulation during the interval of $t = 0-15$ ps, (b) coefficients $|\alpha_1/\Delta|$ and $|1/\Delta|$, (c) absolute value of the coupling coefficient $|\alpha_1|$, and (d) overlapping parameter $G_3(2861, 2861, i)$ defined in eq 9.

In the above paragraph, we have described the frequency rule in the Fermi resonance for the energy transfer. However, the frequency rule is a necessary condition only for the energy transfer and is not a sufficient condition. Because of the high density of modes due to the large number of degrees of freedom in myoglobin, many modes, besides the modes described above, satisfy the resonance condition. Among these numerous modes, the factor selecting the target mode for the energy transfer is the coupling coefficients α and β. As seen in eq 6, the amount of resonance energy is determined by the prefactor α/Δ_0, not $1/\Delta_0$ itself. Here, we will examine the correlation between the value of α/Δ_0 and the energy transferred in the MD simulation.

Before going further, we have to consider the fact that the value of the energy transfer is kept finite even when Δ_0 comes close to zero. When expanding eq 6 to higher orders of α, we realize that $\Delta_0 (= \omega_i - \omega_j)$ should be replaced by the difference in the modulated frequencies, $\Omega_i - \Omega_j$. In other words, we have to evaluate the contribution of the higher order of α in such a way that $\Delta = \Delta_0 + k_1\alpha + k_2\alpha^2 + \cdots$. However, it is difficult to calculate the values of κ_i because of the initial condition dependence of κ_i. Instead, we derived a model for Δ from an analysis of the simulation results in the form of

$$\Delta = \sqrt{\Delta_0^2 + \delta^2} \tag{8}$$

where δ was estimated to be 1.0 cm^{-1} (data not shown). In the following discussion, we will use α/Δ instead of α/Δ_0.

In Figure 3a and b, the simulation results are compared with the theoretical expectation of eq 6 for type 1 resonance. Figure 3a shows the maximum values of the total energy observed in the MD simulation during the interval of $t = 0-15$ ps for mode i near resonance mode 5858. The absolute values of the coefficient in eq 6, $|\alpha_1/\Delta|$, are shown in Figure 3b together with the values of $|1/\Delta|$. The values of α_1 were calculated numerically by differentiating the potential energy, V, or $\partial^3 V/\partial q_{2861}^2 \partial q_i$, and the modulated frequency differences, Δ, were estimated by eq 8. Good agreement between the maximum values of the total energy and $|\alpha_1/\Delta|$ demonstrates that the energy transfer near zero temperature is well described by the resonance scheme of eq 6 (i.e., the energy is transferred to modes having small values of the modulated frequency difference Δ and large values of the coupling coefficient α_1).

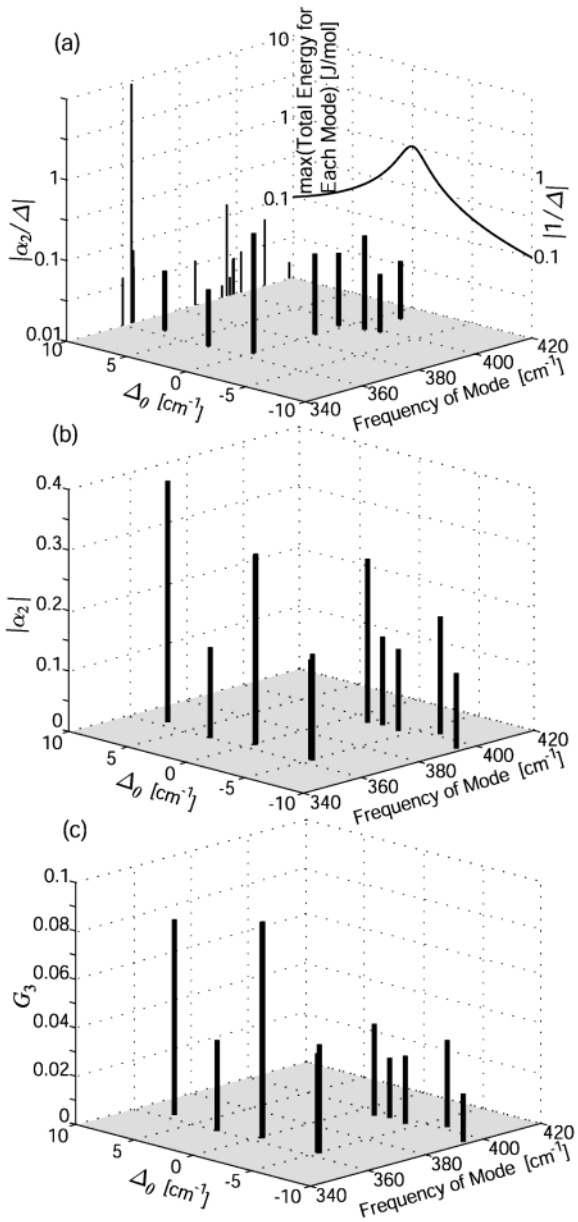

Figure 4. Comparison of various quantities for the energy transfer of type 2 from mode 2861 to modes i and j in the plots relative to the frequency of mode i, ω_i, and the residual of the resonance condition, $\Delta_0 = \omega_{2861} - \omega_i - \omega_j$. (a) Absolute value of the coefficient for the type 2 coupling term, $|\alpha_2/\Delta|$. For the sake of clarity, the values below 0.03 are not plotted. The left upright panel shows the maximum of the total energy, $\max E_i^{2861}(0, t)$, observed in the simulation during the interval of $t = 0-15$ ps. The values of $|1/\Delta|$ are shown in the right upright panel. (b) Absolute value of the coupling coefficient $|\alpha_2|$. (c) Overlapping parameter $G(2861, i, j)$ defined in eq 9.

The energy transfer of type 2 is also well described by the factor $|\alpha_2/\Delta|$. Figure 4a compares the simulation result with the theoretical estimation. The left upright panel shows the maximum of the total energy observed in the MD simulation

during the interval of $t = 0-15$ ps for mode i near resonance mode 1589. The absolute values of the coefficient, $|\alpha_2/\Delta|$, were plotted for the two variables—the frequency of mode i, ω_i, and the residual of the resonance condition, $\Delta_0 = \omega_{2861} - \omega_i - \omega_j$. The values of $|1/\Delta|$ are also shown in the right upright panel. Good agreement was found between of the total energy and $|\{\alpha_2\}/\{\Delta\}|$ and indicates that the resonance scheme of eq 6 is also valid in a type 2 case.

Here, let us consider the structural implication of the mode coupling. We defined the following quantity to measure the geometrical overlap of modes p, q, and r

$$G_3(p,q,r) = \sum_{i=1}^{N_{\text{atom}}} m_i^{3/2} |\mathbf{v}_{ip}||\mathbf{v}_{iq}||\mathbf{v}_{ir}| \tag{9}$$

where N_{atom} is the number of atoms in myoglobin (= 2475) and $\mathbf{v}_{ip}$ is the 3D vector of the eigenvector component for mode p and atom i. Figure 3c and d and Figure 4b and c show excellent agreement between the absolute values of the coupling coefficients, $|\alpha_1|$ and $|\alpha_2|$, and their corresponding G values and lead us to the conclusion that that the coupling coefficients are determined mostly by the geometric overlap of the corresponding normal modes.

The conclusion derived for the third-order coupling can be extended directly to the energy transfer through the fourth-order coupling terms $\beta_3 q_{2861}^3 q_i$ (type 3) and $\beta_4 q_{2861}^2 q_i^2$ (type 4). The resonance condition required for both of the resonance types is $\Delta_0 \equiv w_{2861} - w_i \approx O(\beta)$. Figure 5a−c shows that the two types of coupling terms, type 3 and type 4, concomitantly work to transfer vibrational energy, and Figure 5d−g illustrates good agreement between the absolute values of the coupling coefficients, $|\beta_3|$ and $|\beta_4|$, and the corresponding geometric overlap parameters, G_4, which are calculated in a manner similar to that used in eq 9. It is interesting that the energy transferred to mode 2860 is the largest even though the coupling coefficient is smaller than that of mode 2869 (830.3 cm^{-1}), as shown in Figure 5d and f. This is because the factor $1/\Delta$ representing the resonance condition dominates the contribution of the coupling coefficients, β_3 and β_4, in this case.

3.2. Energy Transfer at Finite Temperatures. In the system near zero temperature, all modes are almost freezing at the minimum-energy structure or have near-zero amplitude except those participating in the energy transfer. Therefore, it is possible to observe the energy transfer through the resonance mechanism requiring a long time without disturbance from the off-resonance coupling. However, in the environment at a finite temperature where all of the modes are oscillating, the perturbed energy will dissipate to the other modes through the off-resonance coupling in a much shorter time before the resonance-type transfer is completed. This is the picture of the temperature dependence of the energy transfer, derived from the model system of two oscillators in section 2.2. To confirm this picture in a large system, myoglobin, we carried out the same MD simulation as that in section 3.1 but at finite temperature or under the condition of all modes being oscillating.

To differentiate the transferred energy from the thermal noise at finite temperatures, we calculated the average excess energy, $\Delta\bar{E}_i^k(T)$, for a given perturbation defined by

$$\Delta\bar{E}_i^k(T) = \langle |E_i^k(T; t; m) - E_i(T; t; m)| \rangle \tag{10}$$

where $E_i(T; t; m)$ is the kinetic energy for mode i at time t calculated from the mth MD trajectory at temperature T and $E_i^k(T; t; m)$ is kinetic energy calculated from the same trajectory but with the perturbation in which a certain amount of kinetic energy is added to mode k at $t = 0$. Here, we used the kinetic energy instead of the total energy because the harmonic approximation of the potential part, $\sum_i[(\omega_i^2 q_i^2)/2]$, breaks down at higher temperatures. The angular bracket means the average in terms of the two variables, t and m. The time average smoothes out the sinusoidal time dependence of the energy. The average in terms of many MD trajectories of various initial conditions, coordinates, and momenta at $t = 0$ reduces the initial condition dependence of the average excess energy.

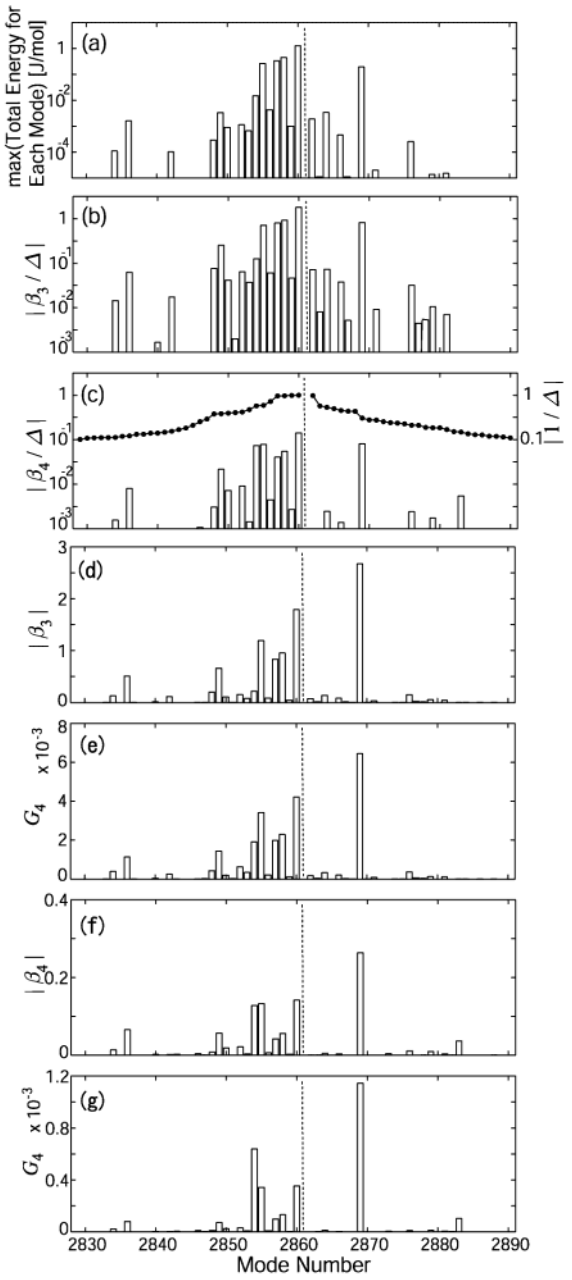

Figure 5. Comparison of various quantities for energy transfers of types 3 and 4 plotted against the mode number around perturbed mode 2861 indicated by the vertical broken line. (a) Maximum of the total energy observed in the simulation during the interval of $t = 0-15$ ps. (b) Coefficient $|\beta_3/\Delta|$. (c) Coefficients $|\beta_4/\Delta|$ and $|1/\Delta|$. (d) Absolute value of the coupling coefficient $|\beta_3|$. (e) Overlapping parameter for type 3 resonance, G_4(2861, 2861, 2861, i). (f) Absolute value of the coupling coefficient $|\beta_4|$. (g) Overlapping parameter for the type 4 resonance, G_4(2861, 2861, i, i).

Figure 6a plots the average excess energy for resonance mode 5858, $\Delta\bar{E}_{5858}^{2861}(T)$ for the perturbation of kinetic energy of 1

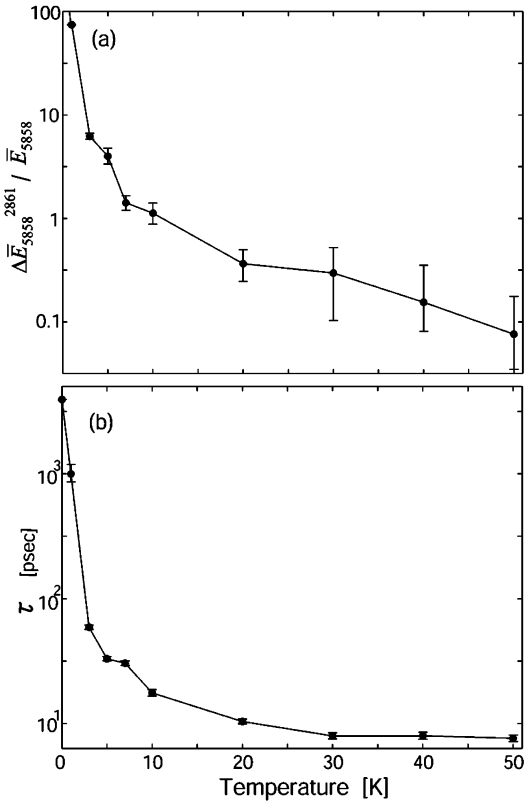

Figure 6. (a) Absolute value of the average excess kinetic energy for mode 5858 averaged over the initial 10-ps trajectory after the perturbation of 1 kcal/mol of kinetic energy to mode 2861. This value was averaged for the results of 100 simulations and normalized by the average kinetic energy of mode 5858 at each temperature, T. (b) Relaxation time, τ, for the sum of the average excess kinetic energy of modes 2861 and 5858 plotted as a function of temperature.

kcal/mol imposed on mode 2861 versus the simulation temperature on the scale normalized by the average kinetic energy of mode 5858 at each temperature, T. The values of $\Delta\bar{E}_{5858}^{2861}(T)$ were averaged during $t = 0-10$ ps and averaged for 100 trajectories calculated with 100 different initial structures sampled from a trajectory of a 100-ps preliminary run at each temperature with an interval of 1 ps. As the temperature increases, the average excess energy quickly decreases to the level of the thermal fluctuation. At 50 K, the resonance contribution has almost disappeared. This result indicates that the energy transfer occurs through the resonance scheme only near zero temperature and that the off-resonance scheme starts to dominates the energy transfer when elevating the temperature slightly from zero.

This switch of the mechanisms from resonance to off-resonance with increasing temperature can also be seen in the relaxation time, τ, of the energy transfer, shown in Figure 6b. The relaxation time, τ, was calculated by fitting the time course of the sum of kinetic energy for modes 2861 and 5858, $\langle E_{2861}^{2861}(T; t) + E_{5858}^{2861}(T; t)\rangle$, during $t = 0-10$ ps to a single-exponential function of t. At ~0 K, the resonance between modes 2861 and 5858 keeps the total kinetic energy constant and results in a very large value of τ (3.9 ns). The finite value of τ indicates that there is a small but not negligible off-resonance-type energy flow from the perturbed mode to modes other than 5858 even at ~0 K. On increasing the temperature only up to 1 K, the kinetic energy starts to dissipate quickly, and at 10 K, the relaxation time decreases by two orders of magnitude (18 ps) over that at ~0 K.

Now we consider the off-resonance energy transfer at temperatures greater than 50 K. The values of the average excess energy shown in Figure 6a, $\Delta\bar{E}_{5858}^{2861}(T)$, can be understood to be the accumulation of the indirect transfers via a number of intermediate modes during 10 ps in addition to the direct transfer from mode 2861. With increasing temperature, such indirect transfers weaken the specificity in the energy transfer between a pair of modes directed by the coupling constant and finally have no distinction from the thermal conduction that produces the equipartition of kinetic energy. This situation prevents us from analyzing the simulation data in more detail on the basis of the model of the coupled harmonic oscillators of eq 1. To avoid this difficulty, we calculated the energy transfer in the short-time limit (1 fs in the present study) with the help of eq 7, which eliminates the possibility of indirect transfer, to obtain the average excess energy for each mode, $\Delta\bar{E}_i^{2861}(T)$, at even higher temperatures. The simulation within 1 fs can cover only an infinitesimal area of the potential surface, unlike the simulations on a longer time scale exploring the rugged potential surface. In this sense, the simulation of the energy transfer within 1 fs investigates the shape of the local potential surface around an instantaneous structure experienced at a finite temperature. Therefore, it is reasonable to analyze the results of such simulations from the viewpoint of the series expansion of the potential-energy-like eq 1.

MD simulations were carried out at 13 different temperatures ranging from 5 to 300 K with a perturbation of 0.1 kcal/mol of kinetic energy added to mode 2861 and with the time step of 0.1 fs to follow the short-time dynamics precisely. The excess kinetic energy, $\Delta\bar{E}_i^{2861}(T)$, was averaged within the interval of $t = 0-1$ fs (or only 10 MD steps after the perturbation). To cover the small number of samples, we repeated the MD simulations 500 times with 500 different initial conditions taken from trajectories of 500-ps preliminary runs at each temperature with an interval of 1 ps. In the analyses of the trajectories, we could successfully calculate the average excess energy even at 300 K.

Figure 7a plots the sum of the average excess energy for all of the modes other than 2861, $\sum_{i\neq 2861}\Delta\bar{E}_i^{2861}(T)$, versus temperature. It is seen that the simulation results exhibit a sudden increase in the gradient at ~180 K. The inflection of the average excess energy at ~180 K reminds us of the glass-transition-like phenomena of protein dynamics,[13−17] which is a dynamic transition from harmonic vibration to anharmonic diffusive motions at around 200 K and has been observed in the inflection in the Debye−Waller factor of incoherent scattering from various proteins including myoglobin.[13,14,31] Also in the MD simulations of myoglobin,[32,33] an inflection in the mean-square fluctuation was found at ~200 K irrespective of the hydration state.

To clarify the relation between the inflection appearing in the transferred energy and the glass transition, we analyzed the simulation results in Figure 7a from the following two aspects. First, we recalculated the energy transfer by reducing the variety of initial structures for the MD simulations. The average excess energy was calculated using the results of 100 simulations with 100 different initial structures taken from the first 100-ps trajectory instead of the full 500-ps trajectory. To avoid an insufficient sampling of initial structures, 100-ps MD simulations were performed 5 times to generate 500 samples. This analysis is based on the following expectation. Within 100 ps, even above the glass-transition temperature, there is a large probability that a myoglobin molecule stays at the same basin of the conformational substate, which can well be represented by the original set of normal modes in the quasiharmonic sense. However,

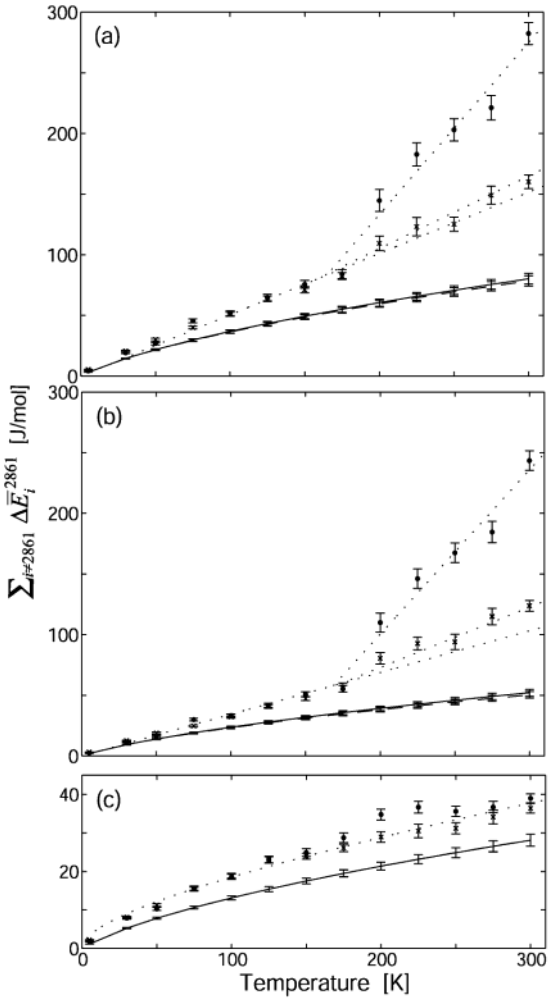

Figure 7. (a) Sum of the absolute values of the average excess energy over all modes, other than mode 2861, averaged over the 500-ps trajectories (●) and the five sets of the first 100-ps trajectories (×) plotted as a function of temperature with error bars. The dotted lines are linear least-squares fittings of those points. The same value calculated by simulating models of harmonic oscillators with the fourth-order coupling and only the third-order coupling are given by solid and broken curves, respectively. See the text for the details. (b, c) Absolute values of the average excess energy averaged for the lower-frequency modes whose frequencies are less than 1640 cm^{-1} and for the bond-stretching modes whose frequencies are greater than 1640 cm^{-1}. The dotted lines in b and the curve (= ~1.4 $T^{1/2}$) in c are the best fits to the data. The same values by model simulation with up to the fourth order and the third order only (see the text for details) are also given in solid and broken curves with error bars, respectively.

during 500 ps, a myoglobin molecule would jump into another substate, which should be represented by a new set of normal modes. When we try to represent the dynamics in the new conformational substate by the original set of normal modes, we have to add many coupling terms to explain the change in the mode space from the original set to the new set. Such coupling terms do not necessarily represent the real energy transfer but rather an artifact caused by the change in the mode space. This expectation was confirmed in Figure 7a, which plots the average excess energy for the first 100-ps trajectory and shows no obvious inflection at ~180 K. Therefore, we conclude that the inflection of the average excess energy at ~180 K is caused by the changes in the mode space due to a jump to a new conformational substate occurring above the glass-transition temperature. Below the transition temperature, the data for the full 500 ps and those for the first 100 ps show good agreement because the system stays at a single conformational substate. In the following discussion, we will use the 100-ps data for the average excess energy.

Second, we separated the sum of the average excess energy into the energy transferred to the lower-frequency modes (<1640 cm^{-1}) and the energy transferred to the higher-frequency modes or the bond-stretching modes (≥1640 cm^{-1}). The results are shown in Figure 7b and c. The energy transfer to the lower-frequency modes clearly exhibits an inflection as shown in Figure 7a, whereas the energy transfer to the bond-stretching modes does not. This suggests that the change in the mode space occurred mostly in the lower-frequency modes rather than in the bond-stretching modes. In Figure 7b and c, the average excess energy for the first 100-ps trajectory shows no obvious inflection either in the transfer to the lower-frequency modes or in the transfer to the bond-stretching modes, as in the corresponding data of Figure 7a. The difference in the energy transfer between higher- and lower-frequency modes can also be seen in the temperature dependence. The energy transfer through the coupling term $q_1^m q_2^n$ (q_1 and q_2 represent the perturbed mode and an energy-receiving mode, respectively) has a temperature dependence whose leading term at high temperature has the form $T^{n/2}$ (Appendix). Because the simulation curve in Figure 7c is well described by the curve of $1.4T^{1/2}$, the leading term of the energy transfer in this frequency region would be $q_1^m q_2$, particularly the term with $m = 2$. However, the simulation curves in Figure 7b appear to be linear relative to temperature. Such a linear dependence may originate from the term proportional to T and from the cancellation between $T^{1/2}$ and $T^{3/2}$. Therefore, the higher-order coupling terms, $q_1^m q_2^2$ and $q_1^m q_2^3$, would make significant contributions to the energy transfer in the lower-frequency modes.

Furthermore, we tried to decompose the values of $\sum_{i\neq2861}\Delta\bar{E}_i^{2861}$ (T) into the contributions from various coupling terms in eq 1 by simulations of a model system, as in the model simulations of Figure 2. In this case, however, the system is far more complicated. The system contains N (= 7419) harmonic oscillators, whose frequencies are those of the normal modes of myoglobin and couple with mode 2861 through the $[(N-1)(N-2)]/2$ third-order coupling terms and through a part of the fourth-order terms, whose coefficients α_{2861ij} and $\beta_{2861ijk}$ in eq 1 were calculated numerically. Since it is not possible to calculate all of the N^3 fourth-order terms, we used the following fourth-order terms in the model: all of the terms $\beta_3 q_{2861}^3 q_i$ (type 3), $\beta_4 q_{2861}^2 q_i^2$ (type 4), $\beta_{2861,i^3} q_{2861} q_i^3$, and $\beta_{(2861)^2ij} q_{2861}^2 q_i q_j$ ($i \neq j$) and 4 268 893 terms $\beta_{2861ijk} q_{2861} q_i q_j q_k$ ($i, j, k \neq 2861$). The last terms were chosen so that at least two of the corresponding third-order coupling coefficients, α_{2861ij}, α_{2861jk}, and α_{2861ik}, are larger than 0.08% of the maximum value of $\alpha_{2861mn}(m \neq n)$. The 4 268 893 terms would explain 14% of the sum $\sum_{i,j,k}|\beta_{2861ijk}|$ according to the inference from the distribution of 100 000 randomly selected coupling coefficients. The total number of coupling terms amounts to almost 6.0×10^{10}. This system mimics a myoglobin molecule without coupling terms higher than fourth order. The simulation was repeated 100 times while changing the initial condition randomly. As a reference, we carried out the same simulations but included only the third-order coupling terms.

The results are also plotted in Figure 7a−c. At low temperatures below 50 K, this model explains the energy-transfer behavior almost perfectly. However, with increasing temperature, the model starts to deviate from the simulation results, particularly in the lower-frequency region (<1640 cm^{-1}). At 300 K, the amount of transferred energy explained by the model is about 50% of the simulation values in the lower-frequency region but about 80% in the bond-stretching motions. This trend

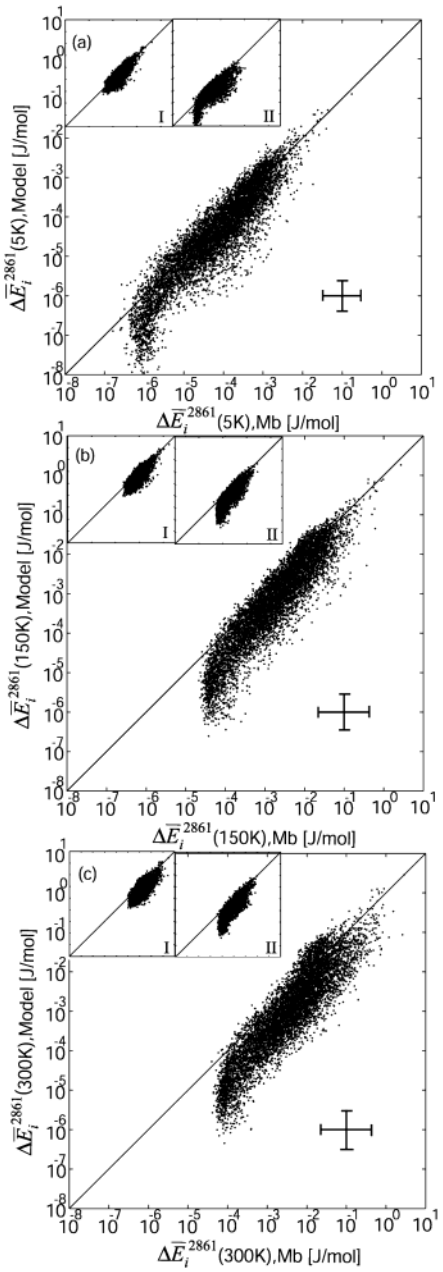

Figure 8. Log−log scattered plots of $\Delta\bar{E}_i^{2861}(T)$, Mb for myoglobin and $\Delta\bar{E}_i^{2861}(T)$, model for the coupled oscillator model for all modes at temperatures of (a) 5 K, (b) 150 K, and (c) 300 K. Error bars for the two kinds of excess energy shown in the lower right corner represent the deviations in the excess energy calculated by MD simulations with various initial conditions, which were evaluated on a log scale as $\langle \log(\sigma/\mu) \rangle$, where σ and μ are the standard deviation and the average of the excess energy of each mode and $\langle\ \rangle$ means the average for all modes. The same plots for the modes with $G_2 \geq 0.01$(I) and $G_2 < 0.01$ (II) are shown in the upper left insets for each temperature.

is consistent with the observation above that the bond-stretching motions are less anharmonic. It is also seen that the third-order terms play dominant roles in the energy transfer and that the fourth-order coupling has only a small influence.

The analyses shown above have been based on the sum of the average excess energy, which would mostly represent the behavior of the leading terms or the behavior of the modes having strong coupling to the perturbed mode, or mode 2861. Here, we compared the transferred energy in myoglobin with that in the model of coupled oscillators mode by mode. The results of the comparison are shown in Figure 8. These two sets of average excess energy values are strongly correlated. The correlation coefficients on a log scale are more than 0.9 at the three temperatures; 0.92, 0.91, and 0.91 for 5, 150, and 300 K, respectively. On a normal scale, however, the widths of the distributions are actually very large for both kinds of excess energy and may correspond to the extremely sensitive dependence of the energy transfer on the initial phases. It is seen in the Figure that the magnitudes of the deviations of the two kinds of excess energy (the error bars in each Figure) calculated by MD simulations with different initial conditions, which each should have different phase relations with the other modes, are almost the same order as the widths of the distributions.

It was shown in Figure 7 that, as far as the absolute values are concerned, the coupled oscillator model seemed to be poor at explaining the excess energy of myoglobin at 300 K. However, it was found in Figure 8 that the pattern of energy transfer, or the relative values of the excess energy, could well be described by the coupled oscillator model irrespective of temperature. This means that the characteristic features of the anharmonic potential surface experienced at finite temperature can well be estimated by the lower-order coupling terms evaluated at the minimum-energy structure.

In section 3.1, we have seen that the energy transfer near zero temperature has a high correlation with the geometric overlap of the corresponding modes evaluated by G_n defined in eq 9. Here, we tried the same analysis on the energy transfer at finite temperatures. We divided the modes into two parts in terms of $G_2(2861, i)$—the modes with $G_2(2861, i) \geq 0.01$ and those with $G_2(2861, i) < 0.01$. The results are shown in the insets of Figure 8. It is clearly seen that the modes with larger G_2 values have larger values of the transferred energy and show good agreement, on an absolute scale, between the results of myoglobin and those of the coupled oscillator model. However, the modes with smaller G_2 values show smaller values of the transferred energy and an underestimation in the coupled oscillator model. These results indicate that the geometric overlap or the corresponding lower-order coupling coefficients also play a dominant role in the energy transfer at finite temperatures, even at 300 K. In the case of the energy transfer between modes with low geometric overlap, higher-order coupling terms seem to make greater contributions, as seen in the results of the coupled oscillator model. The average values of the ratio, defined by [the sum of the excess energy contributed from the fourth-order terms]/[that from the third-order terms], were calculated to be 0.013 and 0.105 at 300 K for the mode with $G_2 \geq 0.01$ and those with $G_2 < 0.01$, respectively. The latter shows a contribution of the fourth-order terms that is almost 10 times larger than that of the former. Moreover, we notice that the lower-value end of the distribution at each temperature shows a large underestimation of the transfer energy calculated by the coupled oscillator model. This underestimation may be due to the fact that the fourth-order coupling terms of $\beta_{2861ijk}q_{2861}q_iq_jq_k$ ($i, j, k \neq 2861$) for these modes were completely missing in the model because of the criterion for choosing the fourth-order terms explained above. It is also seen that the contributions from the fourth-order terms are dominant in these modes; the average value of the ratio of the contributions from the fourth-order terms to that from the third-order terms was calculated to be 0.527 for these modes at 300 K. These observations clearly indicate that the energy transfer between modes with low geometric overlap is dominated by the higher-order coupling terms.

In conclusion, we have the following picture of the off-resonance energy transfer at finite temperature. The characteristic features of the elementary process of the energy transfer in the short-time limit can be described well by the model of

coupled harmonic oscillators with the lower-order coupling terms, even at room temperature. During a longer period, the energy transfer occurs as an accumulation of the elementary processes or as the indirect energy transfer via a number of intermediate modes. Above the glass-transition temperature, the protein molecule moves to a new conformational substate. Because of such motions, the mode space rotates to cause apparent mode couplings.

Acknowledgment. This study was supported by a grant to A.K. from MEXT. O.M. acknowledges a research fellowship for young scientists from the JSPS and the La Jolla Interfaces in Science (LJIS) postdoctoral training program supported by the Burroughs Wellcome Fund. The computations were made at the Computer Center of the Institute for Molecular Science in the Center for Promotion of Computer Science and Engineering of JAERI and at the Science of Biological Supramolecular Systems of Yokohama City University.

Appendix

In this Appendix, we derive the analytical equation of the contribution of the coupling terms to the excess energy of eq 10 in the short-time limit.

In the short-time limit, the excess energy due to the third-order coupling term $\alpha_1 q_1^2 q_2$ (q_1 and q_2 represent the perturbed mode and an energy-receiving mode, respectively) can be evaluated by averaging eq 7 in terms of the initial phases of two modes and a time duration of Δt as

$$\Delta\bar{E}_2^1(T) \simeq \frac{|\alpha_1|\delta A_1^2 A_2 \Delta t}{\pi}\omega_2 \tag{A1}$$

where δA_1^2 is the increase in the square of the mode amplitude after the perturbation of kinetic energy, δE^1, is imposed on mode 1 (i.e., $\delta E^1 = (1/2)\delta A_1^2 \omega_1^2$). When A_i is substituted by $A_i = (2k_BT)^{1/2}/\omega_i$ (k_B being the Boltzmann constant), eq A1 becomes

$$\Delta\bar{E}_2^1(T) \simeq \frac{2\sqrt{2}|\alpha_1|\delta E^1 (k_BT)^{1/2}\Delta t}{\pi\omega_1^2} \tag{A2}$$

In the same manner, the excess energy caused by another type of third-order coupling term, $\alpha_2 q_1 q_2^2$, and two types of fourth-order coupling terms, $\beta_3 q_1^3 q_2$ and $\beta_4 q_1^2 q_2^2$, have the following forms, respectively:

$$\Delta\bar{E}_2^1(T) \simeq \frac{8|\alpha_2|\delta A_1 A_2^2}{\pi^2}\omega_2\Delta t = \frac{16|\alpha_2|[(\delta E^1 + k_BT)^{1/2} - (k_BT)^{1/2}]k_BT\Delta t}{3\pi^2\omega_1\omega_2} \tag{A3}$$

$$\Delta\bar{E}_2^1(T) \simeq \frac{8|\beta_3|\delta A_1^3 A_2}{3\pi^2}\omega_2\Delta t = \frac{32|\beta_3|[(\delta E^1 + k_BT)^{3/2} - (k_BT)^{3/2}](k_BT)^{1/2}\Delta t}{3\pi^2\omega_1^3} \tag{A4}$$

$$\Delta\bar{E}_2^1(T) \simeq \frac{|\beta_4|\delta A_1^2 A_2^2}{\pi}\omega_2\Delta t = \frac{4|\beta_4|\delta E^1 k_BT\Delta t}{\pi\omega_1^2\omega_2} \tag{A5}$$

The energy transfer through a coupling term has a temperature dependence whose leading term at higher temperature has the form $T^{n/2}$.

References and Notes

(1) Frauenfelder, H.; Slinger, S. G.; Wolynes, P. G. *Science (Washington, D.C.)* **1991**, *254*, 1598.

(2) Frauenfelder, H.; Parak, F.; Young, R. D. *Annu. Rev. Biophys. Biophys. Chem.* **1988**, *17*, 451.

(3) Kitao, A.; Go, N. *Curr. Opin. Struct. Biol.* **1999**, *9*, 164.

(4) Amadei, A.; Linssen, A. B. M.; Berendsen, H. J. C. *Proteins* **1993**, *17*, 283.

(5) Kitao, A.; Hayward, S.; Go, N. *Proteins* **1998**, *33*, 496.

(6) Moritsugu, K.; Miyashita, O.; Kidera, A. *Phys. Rev. Lett.* **2000**, *85*, 3970.

(7) Bigwood, R.; Gruebele, M. *Chem. Phys. Lett.* **1995**, *235*, 604.

(8) Leitner, D. M.; Wolynes, P. G. *J. Phys. Chem. A* **1997**, *101*, 541.

(9) Pearman, R.; Gruebele, M. *J. Chem. Phys.* **1998**, *108*, 6561.

(10) Bigwood, R.; Grubele, M.; Leitner, D. M.; Wolynes, P. G. *Proc. Natl. Acad. Sci. U.S.A.* **1998**, *95*, 5960.

(11) Austin, R. H.; Beeson, K. W.; Eisenstein, L.; Frauenfelder, H.; Gunsalus, I. C. *Biochemistry* **1975**, *14*, 5355.

(12) Iben, I. E. T.; Braunstein, D.; Doster, W.; Frauenfelder, H.; Hong, M. K.; Johnson, J. B.; Luck, S.; Ormos, P.; Schulte, A.; Steinbach, P. J.; Xie, A. H.; Young R. D. *Phys. Rev. Lett.* **1989**, *62*, 1916.

(13) Doster, W.; Cusack, S.; Petry, W. *Nature (London)* **1989**, *337*, 754.

(14) Smith, J.; Kuczera, K.; Karplus, M. *Proc. Natl. Acad. Sci. U.S.A.* **1990**, *87*, 1601.

(15) Tilton, R. F.; Dewan, J. C.; Petsuko, G. A. *Biochemistry* **1992**, *31*, 2469.

(16) Rasmussen, B. F.; Stock, A. M.; Ringe, D.; Petsuko, G. A. *Nature (London)* **1992**, *357*, 423.

(17) Zaccai, G. *Science (Washington, D.C.)* **2000**, *288*, 1604.

(18) Mizutani, Y.; Kitagawa, T. *Science (Washington, D.C.)* **1997**, *278*, 443.

(19) Lian, T.; Lucke, B.; Kholodenko, Y.; Hochstrasser, R. M. *J. Chem. Phys.* **1997**, *98*, 11648.

(20) Henry, E. R.; Eaton, W. A.; Hochstrasser, R. M. *Proc. Natl. Acad. Sci. U.S.A.* **1986**, *83*, 8982.

(21) Sagnella, D. E.; Straub, J. E. *J. Phys. Chem. B* **2001**, *105*, 7057.

(22) Lingle, R., Jr.; Xu, X.; Zhu, H.; Yu, S.-C.; Hopkins, J. B. *J. Phys. Chem.* **1991**, *95*, 9320.

(23) Li, P.; Sage, J. T.; Champion, P. M. *J. Chem. Phys.* **1992**, *97*, 3214.

(24) Franzen, S.; Bohn, B.; Poyart, C.; Martin, J. L. *Biochemistry* **1995**, *34*, 1224.

(25) Petrich, J. W.; Martin, J. L.; Houde, D.; Poyart, C.; Orszag, A. *Biochemistry* **1987**, *26*, 7914.

(26) Martin, J. L.; Migus, A.; Poyart, C.; Lecarpentier, Y.; Astier, R.; Antonetti, A. *Proc. Natl. Acad. Sci. U.S.A.* **1983**, *80*, 173.

(27) Norikami, K.; Nakai, T.; Kidera, A.; Saito, M.; Nakamura, H. *Comput. Chem.* **1996**, *100*, 2567.

(28) Cornell, W. D.; Cieplak, P.; Bayly, C. I.; Gould, I. R.; Merz, K. M., Jr.; Ferguson, D. M.; Spellmeyer, D. C.; Fox, T.; Caldwell, J. W.; Kollman, P. A. *J. Am. Chem. Soc.* **1995**, *117*, 5179.

(29) Wilson, E. B.; Decius, J. C.; Cross, P. C. *Molecular Vibrations*; McGraw-Hill: New York, 1955.

(30) Sakurai J.; Tuan, S. F. *Modern Quantum Mechanics*; Addison-Wesley: New York, 1995.

(31) Chong, S.-H.; Joti, Y.; Kidera, A.; Go, N.; Ostermann, A.; Gassmann, A.; Parak, F. *Eur. Biophys. J.* **2001**, *30*, 319−329.

(32) Steinbach, P. J.; Brooks, B. R. *Proc. Natl. Acad. Sci. U.S.A.* **1993**, *90*, 9135.

(33) Steinbach, P. J.; Brooks, B. R. *Proc. Natl. Acad. Sci. U.S.A.* **1996**, *93*, 55.